A&A 376, 861–877 (2001)
DOI: 10.1051/0004-6361:20011000

Astronomy & Astrophysics

A radio continuum survey of the southern sky at 1420 MHz

The atlas of contour maps⋆

P. Reich[1], J. C. Testori[2], and W. Reich[1]

[1] Max-Planck-Institut für Radioastronomie, Auf dem Hügel 69, 53121 Bonn, Germany
[2] Instituto Argentino de Radioastronomía, C.C. 5, 1894 Villa Elisa (Prov. de Bs. As.), Argentina

Received 22 May 2001 / Accepted 22 June 2001

Abstract. The results of an absolutely calibrated radio continuum survey of the South Celestial Hemisphere at a frequency of 1420 MHz are presented. Contour maps show the area $0^{\rm h} \leq {\rm RA} \leq 24^{\rm h}$ for the declination range $-90°$ to $-10°$. Contour steps (50 mK $T_{\rm B}$; 3 × rms noise) and angular resolution ($HPBW$ 35.′4) of the maps match the already existing Stockert northern sky survey at the same frequency. We compare flux densities of compact and extended sources with published data from the Parkes 64-m telescope and find excellent agreement in general. The survey maps are sensitive enough to constrain synchrotron and thermal emission components which might influence studies of the cosmic microwave background.

Key words. surveys – Galaxy: general – radio continuum: general

1. Introduction

We present the results of a radio continuum survey of the South Celestial Hemisphere at a frequency of 1420 MHz carried out with a 30-m radio telescope at Villa Elisa, Argentina. In a first paper (Testori et al. 2001, Paper I) we described in detail the telescope, the method of observation, the data acquisition, the reduction procedures and the absolute calibration of the measurements. This radio continuum survey is intended to complement the northern sky survey (Reich 1982; Reich & Reich 1986) made with the 25-m Stockert telescope to an all-sky radio continuum survey at 1420 MHz. The region of overlap between $-10°$ to $-19°$ of both surveys was used to prove their agreement in scale and angular resolution as demonstrated in Paper I.

The main motivation for carrying out this survey was the study of Galactic emission on large scales and the spectral index distribution across the sky as noted in Paper I. Large-scale structures are well represented in this survey because of its absolute calibration and high baseline stability. Integrated flux densities of extended sources can be derived in addition, and we give the results for some objects where flux densities have been previously reported from measurements at the same frequency with the Parkes telescope. Also flux densities of selected compact sources are compared.

Although the rms noise of the survey is about the same as for the Stockert northern sky survey, the quality of the map is much less affected by scanning effects due to improved reduction software, but in particular to the dramatic increase of computing power compared to the situation about 20 years ago when the northern sky data were reduced. Therefore this survey traces the Galactic foreground at high Galactic latitudes, which might influence high-frequency studies of cosmic microwave background fluctuations.

2. Scales and accuracy of the survey maps

A few of the most characteristic parameters of the survey are listed in Table 1. For more details we refer to Paper I. Because of technical reasons or forced by the actual interference situation, the central frequency and bandwidth were slightly changed (numbers in brackets in Table 1) for the different periods of observations. From calibration source measurements we estimate a scale accuracy of about 5%. The zero level was adopted from sky horn measurements as discussed in Paper I, where some discrepancies between different measurements became obvious. This could be sorted out with the help of the 408 MHz all-sky survey by Haslam et al. (1982), however.

We rely on the same full beam brightness scale for the representation of the data as used for the Stockert

Send offprint requests to: P. Reich,
e-mail: preich@mpifr-bonn.mpg.de

⋆ Figures 1 and 2 are also available in electronic form at the CDS via anonymous ftp to cdsarc.u-strasbg.fr (130.79.128.5) or via
http://cdsweb.u-strasbg.fr/cgi-bin/qcat?J/A+A/376/861

Table 1. Observational parameters of the Villa Elisa survey.

Antenna diameter	30 m
HPBW	$35\farcm4$
Centre frequency	1420 (1435) MHz
Bandwidth	13 (14) MHz
Coverage	$0^{\rm h} \le {\rm RA} \le 24^{\rm h}$ $-90^\circ \le \delta \le -10^\circ$
Sensitivity	$\sim$50 mK $T_{\rm B}$ (3 × rms noise)
Gain scale accuracy	5%
$S/T_{\rm B}$ (full beam)	11.25 Jy/K

northern sky. This is the beam solid angle measured to such an extent as to represent the correct brightness temperature for extended emission on about that scale. Because of the limited hour angle range where the Villa Elisa telescope can be moved and the fact that very strong compact sources are missing in the southern sky, we decided to adopt the Stockert "full beam" scale rather than to try an independent antenna pattern measurement.

The Stockert antenna pattern was originally measured by mapping CAS A (Reich 1982) in such a method that it was possible to remove surrounding emission from unrelated objects. The full-beam solid angle measured for an area of 7° in diameter was found to be 83% of the antenna solid angle (Reich & Reich 1988). A 7°-wide "full beam" is rather similar to those adopted for the 408 MHz survey (Haslam et al. 1982) and the 820 MHz survey (Berkhuijsen 1972). This is of relevance when studying the spectral index distribution of the large-scale Galactic emission. However, the ratio between the main-beam and the full-beam efficiency varies for the different surveys (Reich & Reich 1988) and must be taken into account when calculating spectral indices for sources or structures smaller than the full beam extent.

The Villa Elisa 30-m dish was underilluminated to match the Stockert 25-m beam size. Only small differences in the ratio of the full-beam and main-beam temperatures between the two surveys will result. In fact, we have proved in Paper I that the adaptation of the Stockert full-beam scale is relevant. When the same ratio of $S/T_{\rm B}$ (full beam) is applied to the southern sky survey the TT- (Temperature–versus–Temperature) plot of the Villa Elisa data versus the Stockert data for the intense Galactic ridge close to the Galactic center gives a scaling agreement within 2%. The peak temperatures for compact sources measured from both surveys also agree and therefore about the same ratio between the main-beam and full-beam scales of 1.55 as found for the Stockert northern sky survey needs to be adopted. This scaling factor has to be applied to the data when they are compared with maps using the conventional main-beam temperature scale.

The observing method as described in Paper I consisted of moving the telescope in elevation continuously up and down along the meridian. Fully sampled coverages from the up and the down scans of the sky where obtained. The advantage of this procedure is the nearly constant contribution from the ground depending only on elevation, which can be accounted for as described in Paper I and the remaining drift effects can be minimized by appropriate reduction of the common data collected for many nights with different conditions. This mapping technique has successfully been applied before by Reich & Steffen (1981) at 1420 MHz using the Stockert 25-m telescope at low elevations down to 10°. When mapping the northern sky at 1420 MHz, azimuth scans were made. At a constant elevation the contribution from the ground varies much less along a scan than is the case for meridian scans. However, we did not find a significant difference in the accuracy of its determination. A proof of the adapted method comes from spectral index maps made from surveys with different scanning directions, where any residual ground radiation left in the data should show up as a systematic declination dependent effect. This is in fact not present for the 408 MHz and the 1420 MHz northern sky surveys (Reich & Reich 1988). A spectral index map of the southern sky is in preparation, which proves that this holds also for the southern sky survey.

Tello et al. (2000) follow a different observing technique to make maps of the sky at decimeter wavelengths aiming for precise baselines on large scales. They state that it turns out to be essential to shield their 5.5-m dish against ground radiation. Tello et al. (2000) used a wire mesh screen, which in fact improves their 1465 MHz map significantly to that obtained without screen. However, such a shielding is obviously not perfect as seen from their results. A significant temperature gradient in declination is left in the 1465 MHz map (their Fig. 3), which is inconsistent with our map. Available maps at other frequencies of the southern sky do not show such a temperature gradient as well.

3. The atlas of contour maps

The style of the presentation of the survey in the form of contour maps (Figs. 1a to 1l and Fig. 2) closely follows that of the presentation of the Stockert northern sky survey, although larger areas are shown in each figure. Aside from the equatorial coordinates, which we kept at B1950 for an easy comparison with previously published contour maps, we have overlaid a grid of Galactic coordinates in addition. The contours are in full-beam brightness temperature $T_{\rm B}$ and have been absolutely calibrated by sky horn measurements including the cosmic background radiation. Contours run in steps of 50 mK from 3.35 K to 4.8 K, labeled every 0.2 K. Further steps are 80 mK up to 6 K (labeled every 0.4 K) and 250 mK up to 9 K. Labeled contours run from 6 K to 12 K in steps of 1 K, up to 20 K in steps of 2 K. Further steps are 5 K apart (labeled every 10 K). The maximum intensity of the survey is at the Galactic Center where 82 K are measured.

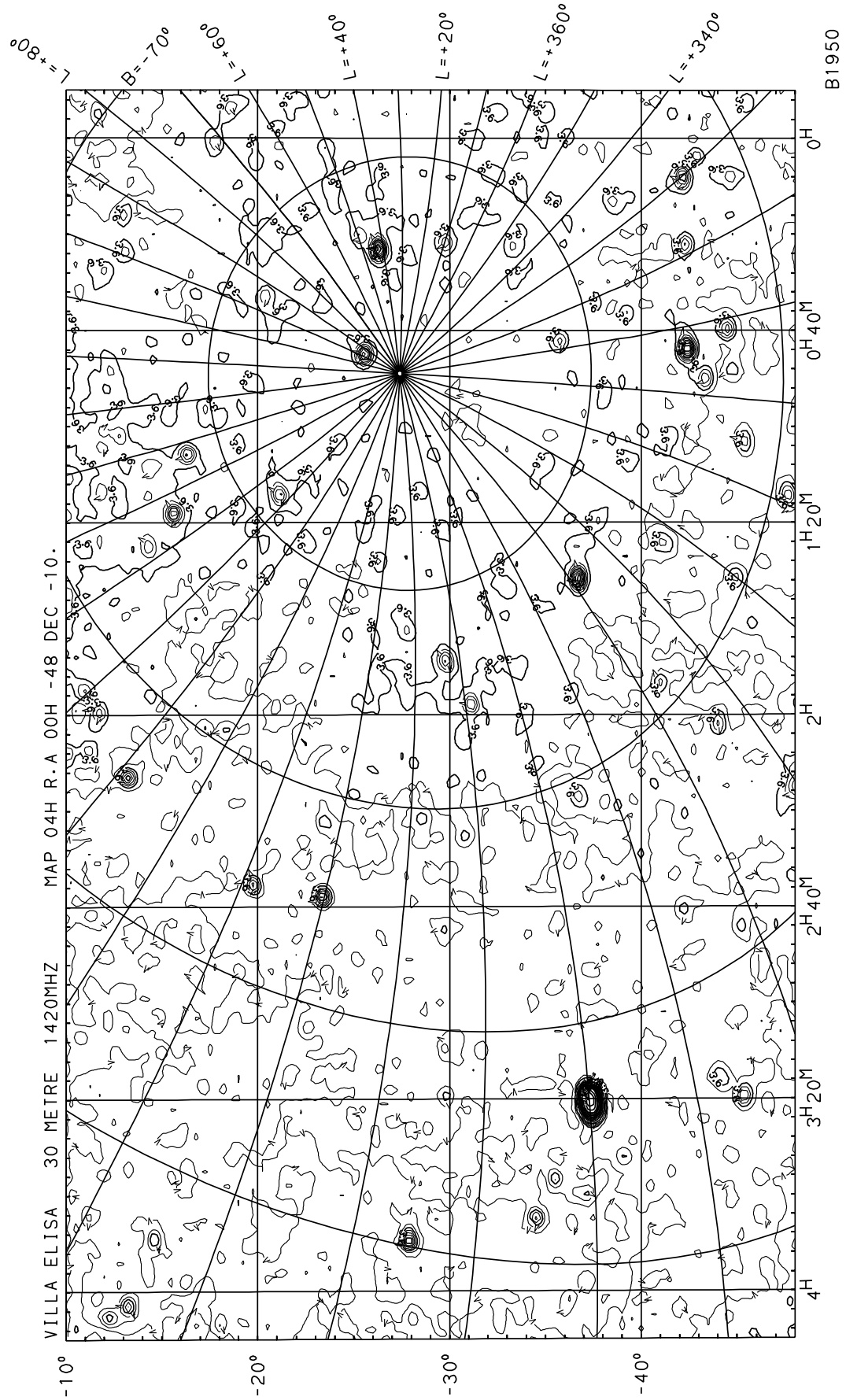

Fig. 1. a). The southern sky survey maps at 1420 MHz. Contour steps are listed in Sect. 3.

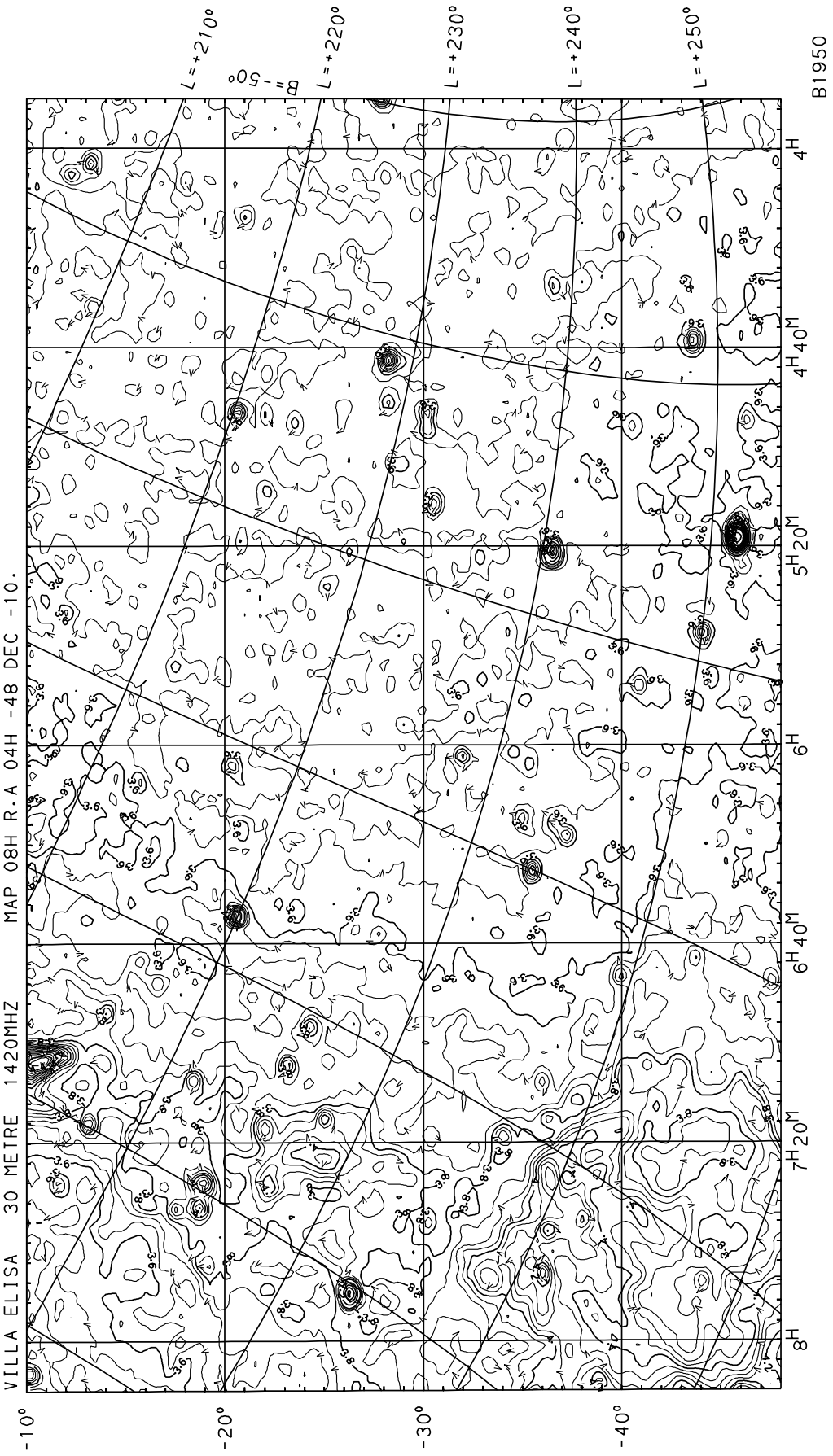
VILLA ELISA 30 METRE 1420MHZ MAP 08H R.A 04H -48 DEC -10.
B1950
L=+210°
L=+220°
L=+230°
L=+240°
L=+250°
B=-50°
-10°
-20°
-30°
-40°
8H
7H20M
6H40M
6H
5H20M
4H40M
4H

Fig. 1. b)

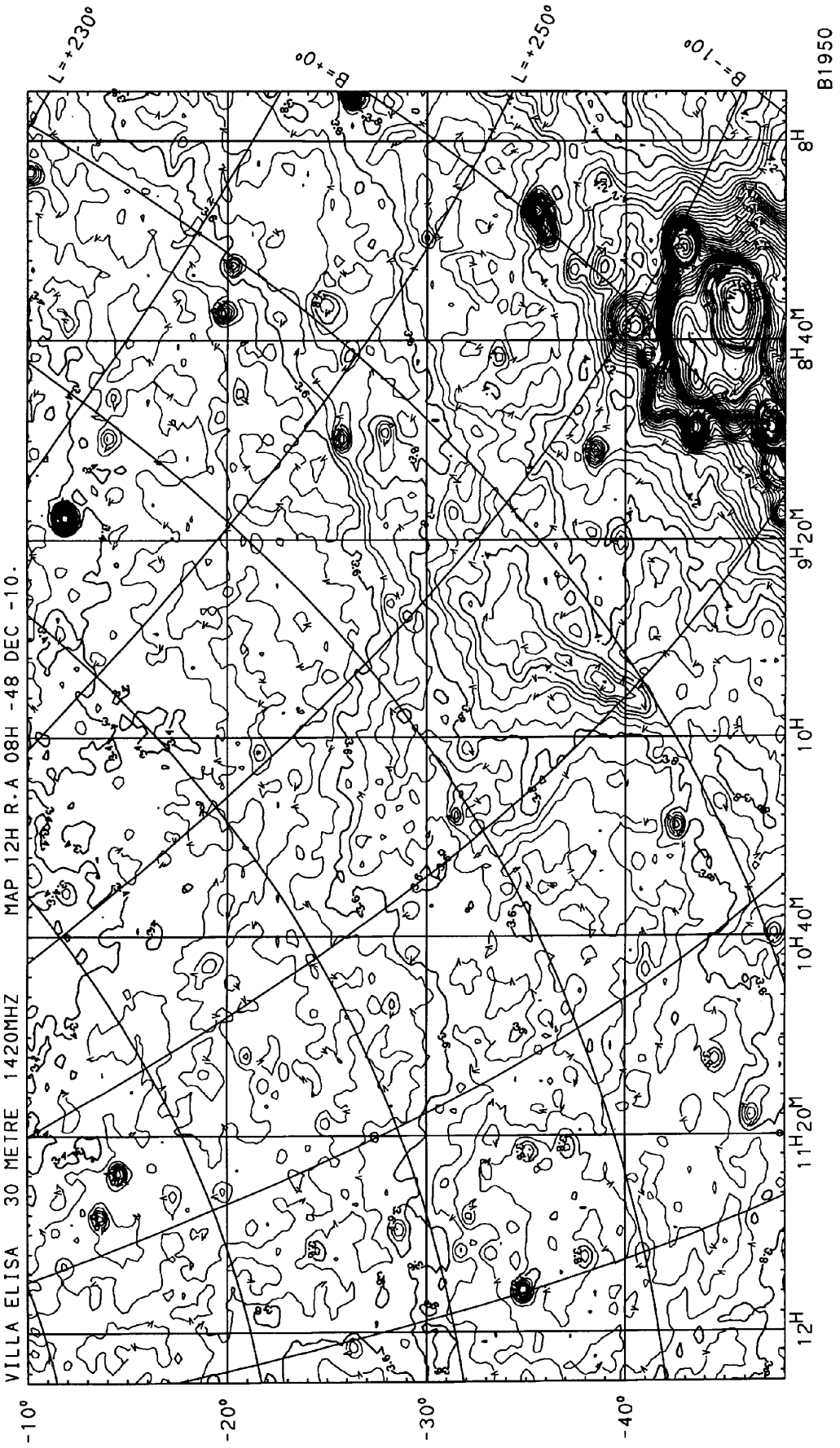
VILLA ELISA 30 METRE 1420MHZ MAP 12H R.A 08H -48 DEC -10.
L=+230°
B=+0°
L=+250°
B=-10°
B1950
8H
8H40M
9H20M
10H
10H40M
11H20M
12H
-10°
-20°
-30°
-40°

Fig. 1. c)

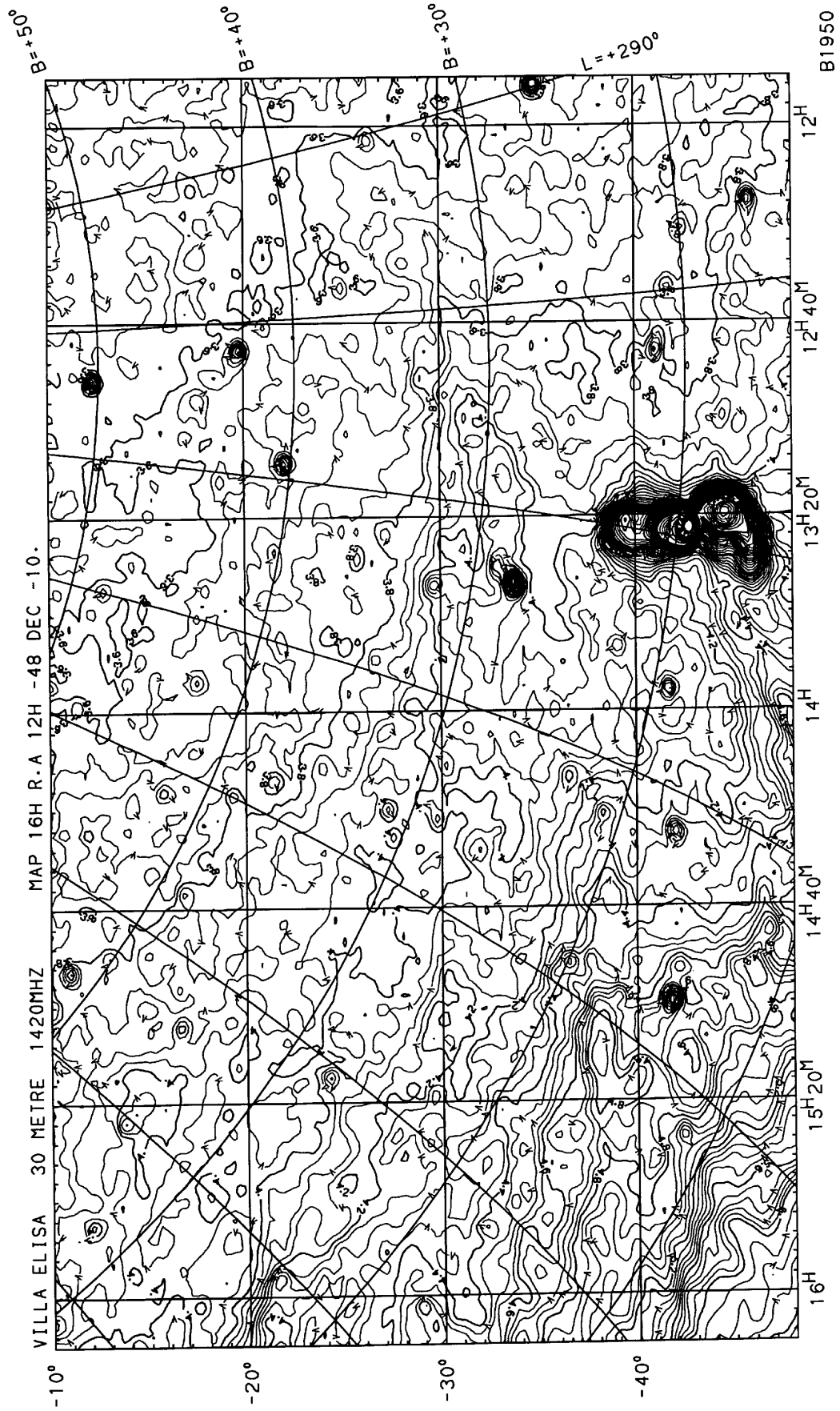
VILLA ELISA 30 METRE 1420MHZ MAP 16H R.A 12H -48 DEC -10.
B=+50°
B=+40°
B=+30°
L=+290°
B1950
12H
12H40M
13H20M
14H
14H40M
15H20M
16H
-10°
-20°
-30°
-40°

Fig. 1. d)

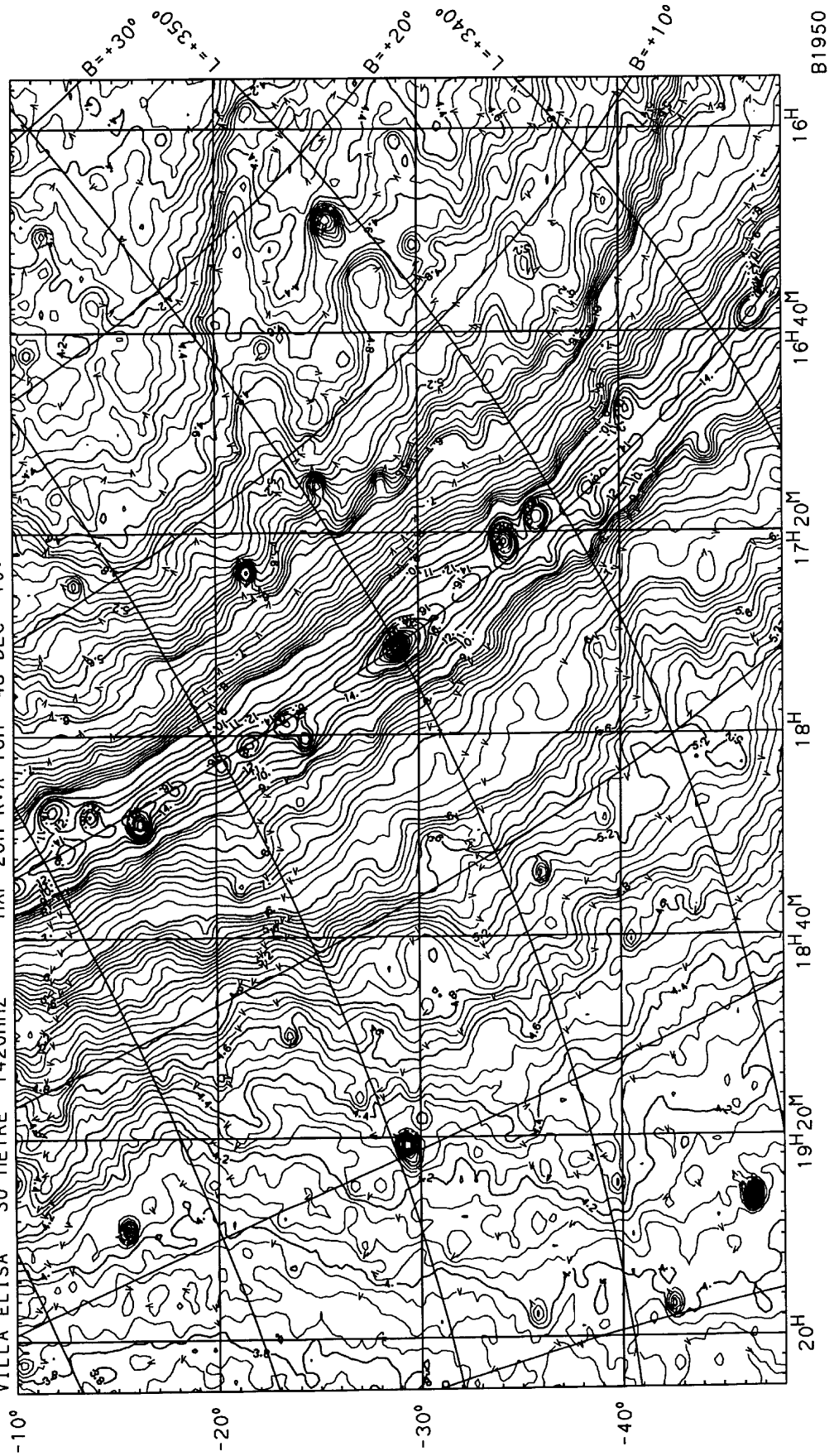
VILLA ELISA 30 METRE 1420MHZ MAP 20H R.A 16H -48 DEC -10.
B1950
B=+30°
L=+350°
B=+20°
L=+340°
B=+10°
16H
16H40M
17H20M
18H
18H40M
19H20M
20H
-10°
-20°
-30°
-40°

Fig. 1. e)

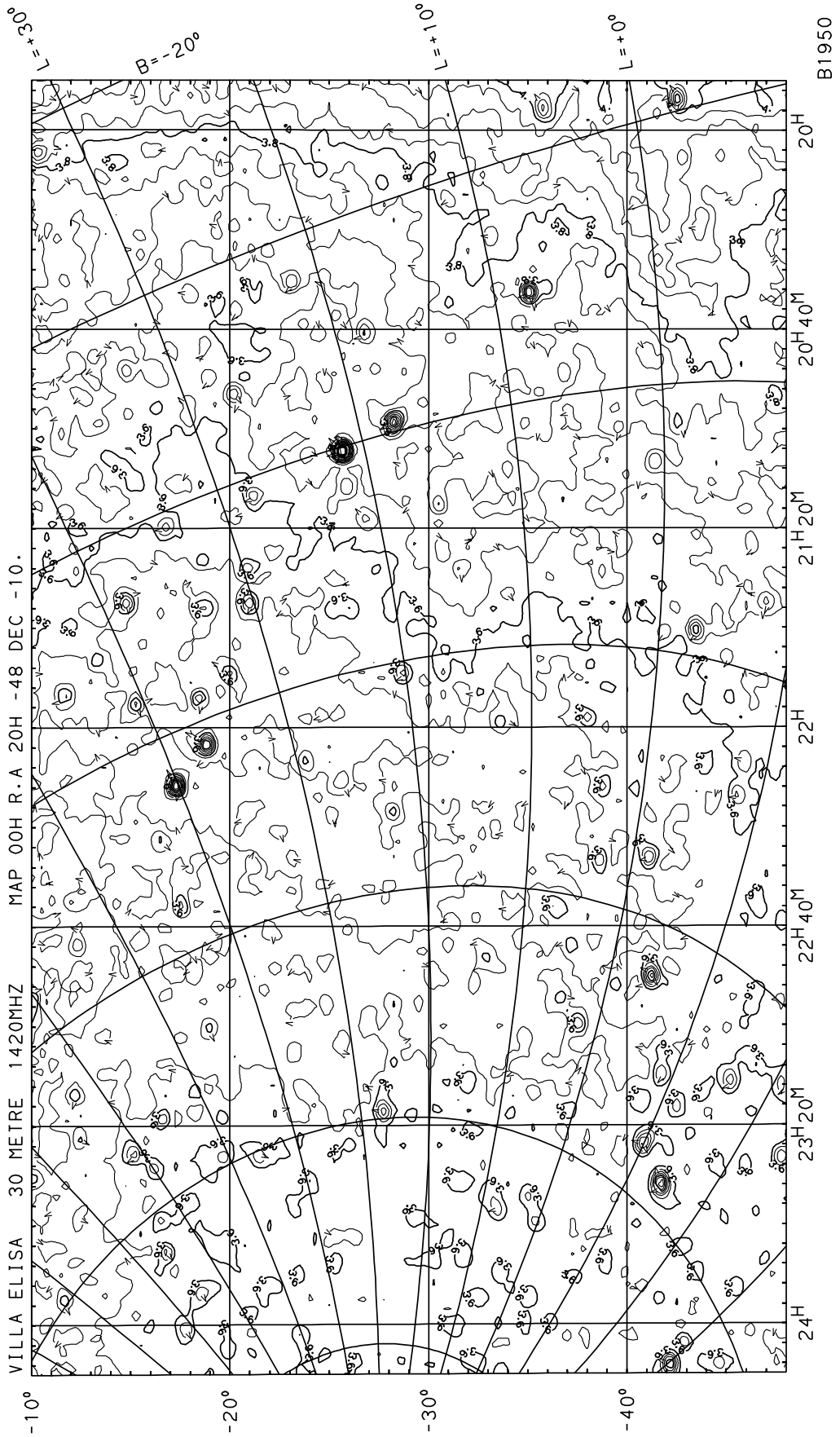
VILLA ELISA 30 METRE 1420MHZ MAP 00H R.A 20H -48 DEC -10.
B=-20°
L=+30°
L=+10°
L=+0°
B1950
20H
20H40M
21H20M
22H
22H40M
23H20M
24H
-10°
-20°
-30°
-40°

Fig. 1. f)

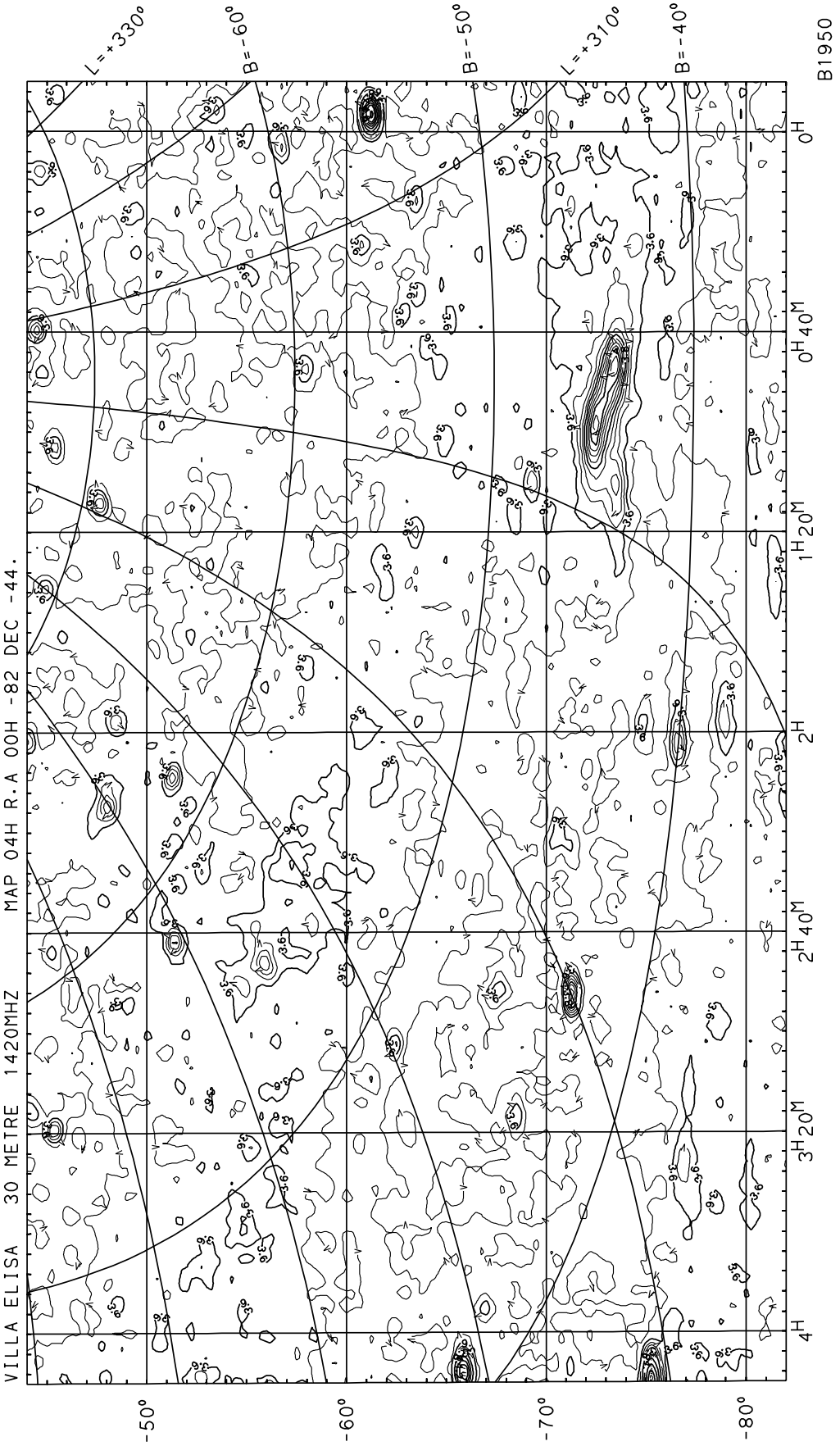
VILLA ELISA 30 METRE 1420MHZ MAP 04H R.A 00H -82 DEC -44.
L=+330°
B=-60°
B=-50°
L=+310°
B=-40°
B1950
0H
0H40M
1H20M
2H
2H40M
3H20M
4H
-50°
-60°
-70°
-80°

Fig. 1. g)

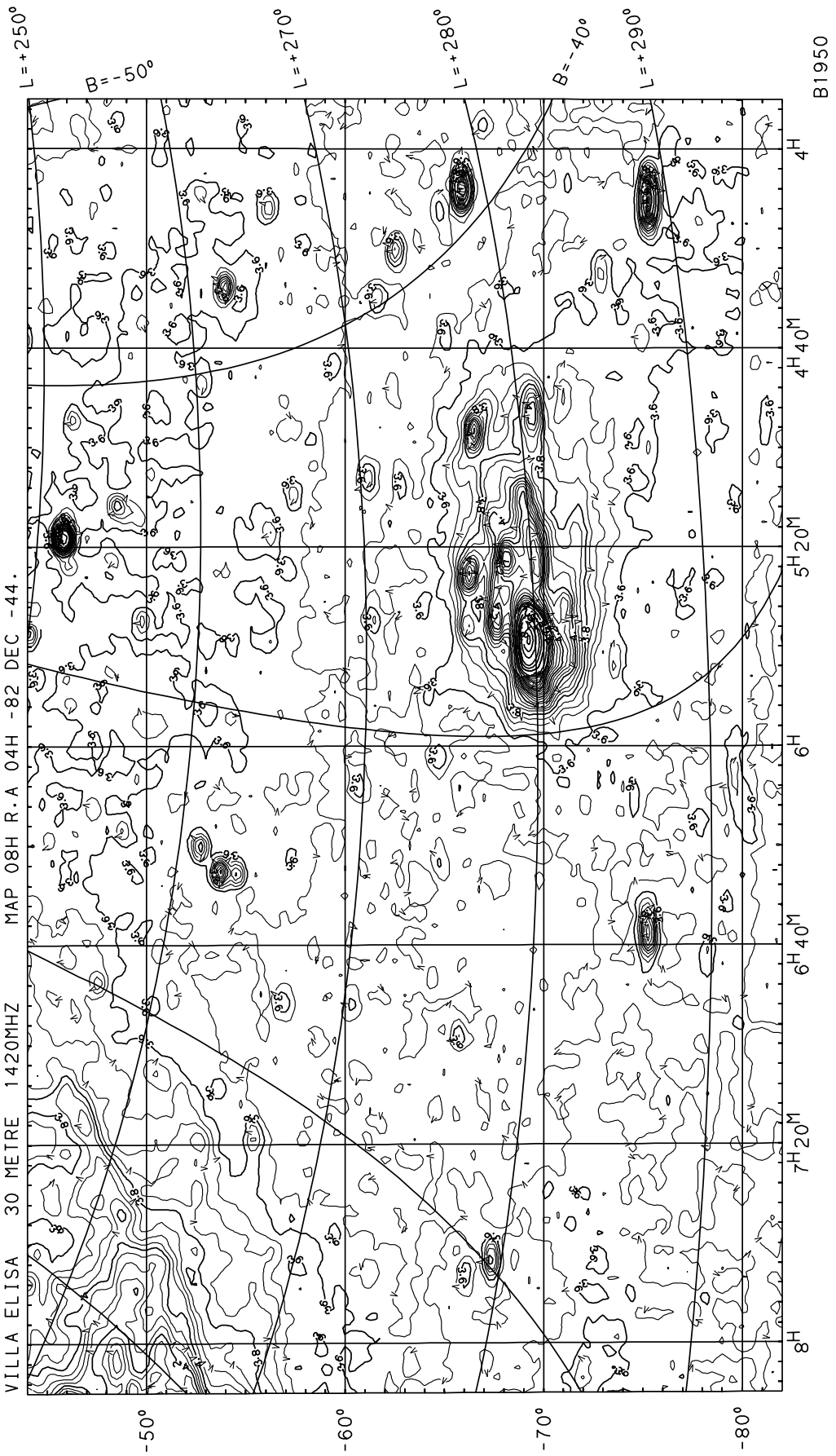
VILLA ELISA 30 METRE 1420MHZ MAP 08H R.A 04H -82 DEC -44.
L=+250°
B=-50°
L=+270°
L=+280°
B=-40°
L=+290°
B1950
4H
4H40M
5H20M
6H
6H40M
7H20M
8H
-50°
-60°
-70°
-80°

Fig. 1. h)

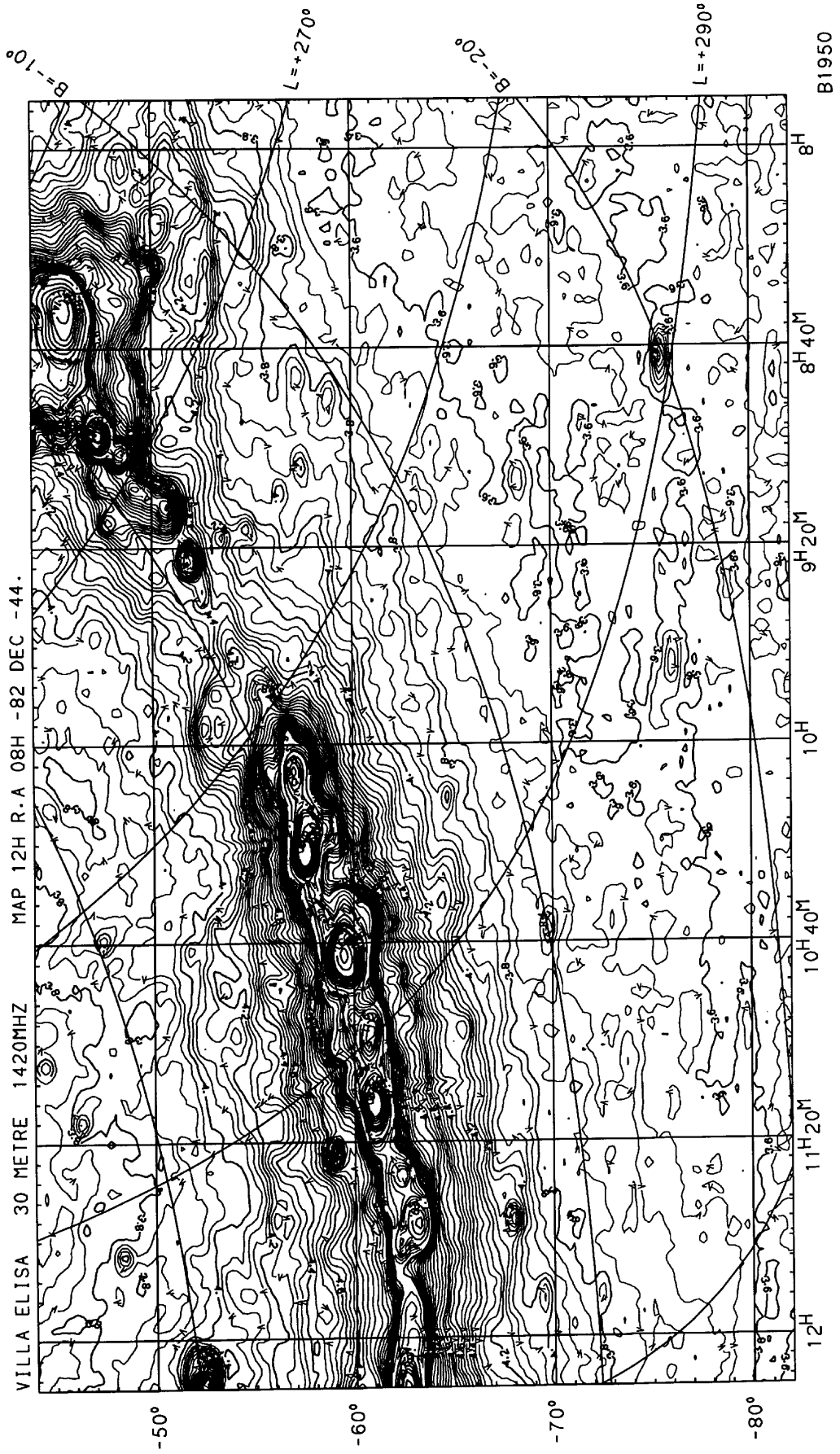
VILLA ELISA 30 METRE 1420MHZ MAP 12H R.A 08H -82 DEC -44.
B=-10°
L=+270°
B=-20°
L=+290°
B1950
8H
8H40M
9H20M
10H
10H40M
11H20M
12H
-50°
-60°
-70°
-80°

Fig. 1. i)

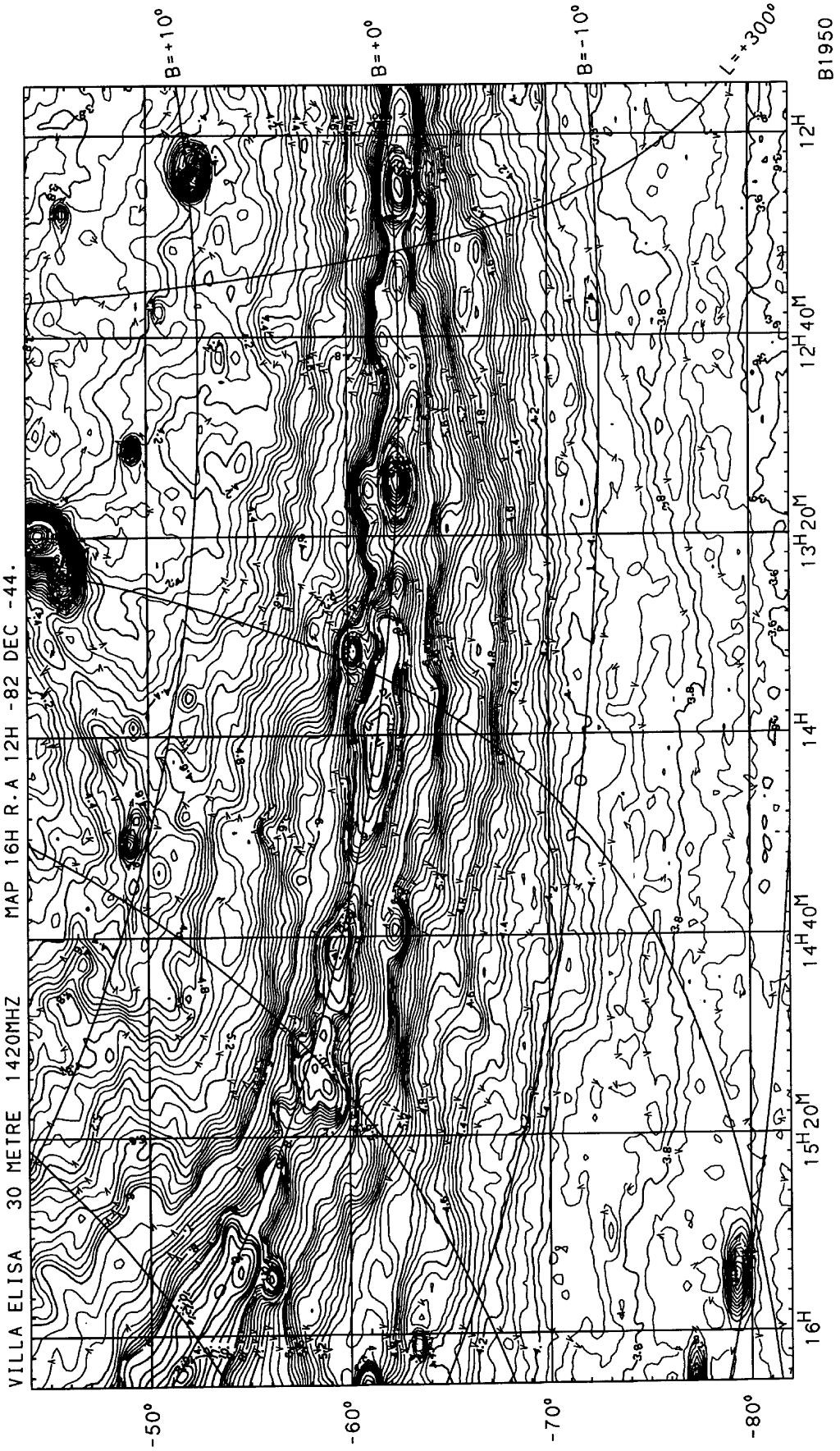
VILLA ELISA 30 METRE 1420MHZ MAP 16H R.A 12H -82 DEC -44.
B=+10°
B=+0°
B=-10°
L=+300°
B1950
12H
12H40M
13H20M
14H
14H40M
15H20M
16H
-50°
-60°
-70°
-80°

Fig. 1. j)

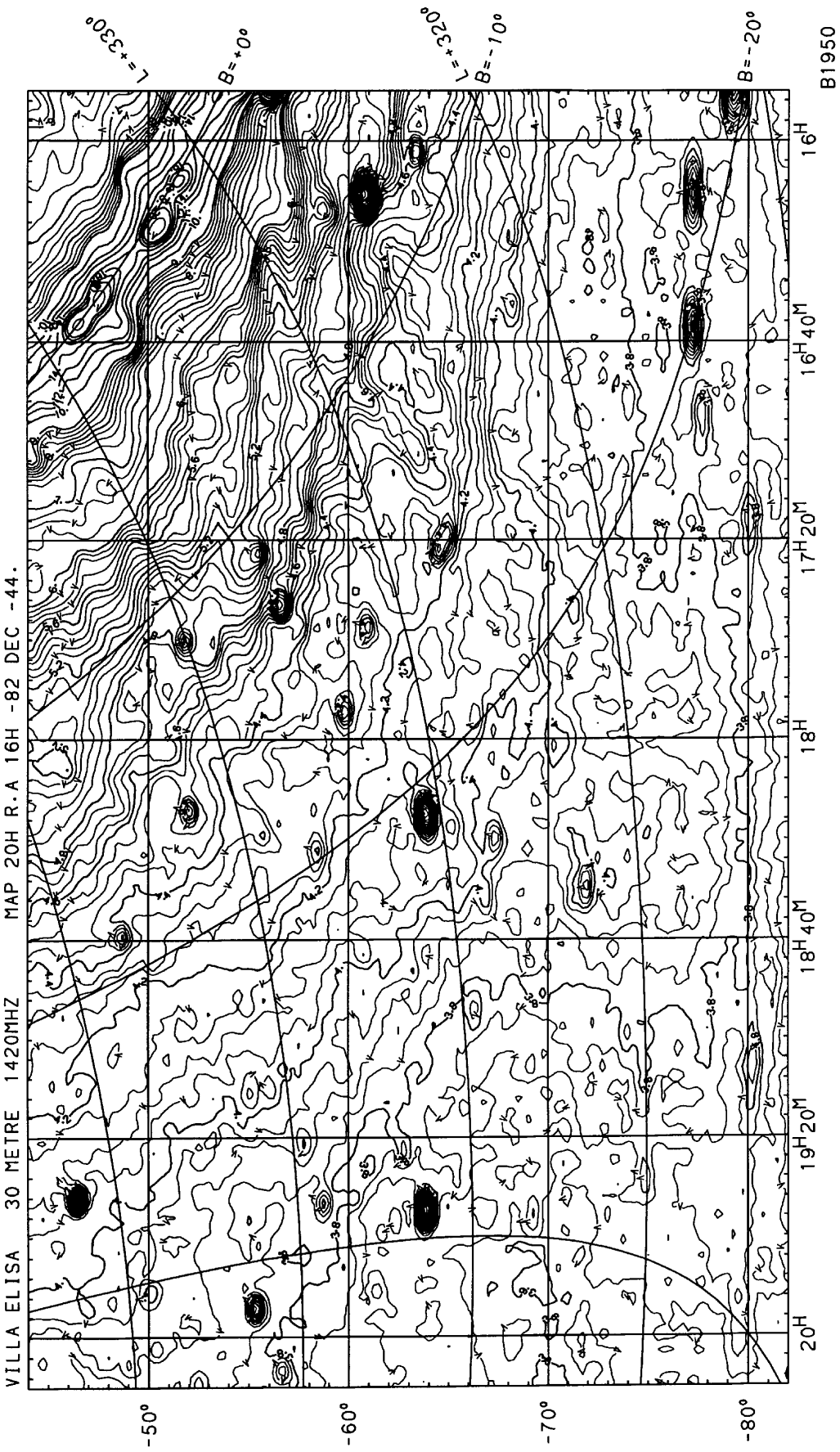
VILLA ELISA 30 METRE 1420MHZ MAP 20H R.A 16H -82 DEC -44.
L=+330°
B=+0°
L=+320°
B=-10°
B=-20°
B1950
16H
16H40M
17H20M
18H
18H40M
19H20M
20H
-50°
-60°
-70°
-80°

Fig. 1. k)

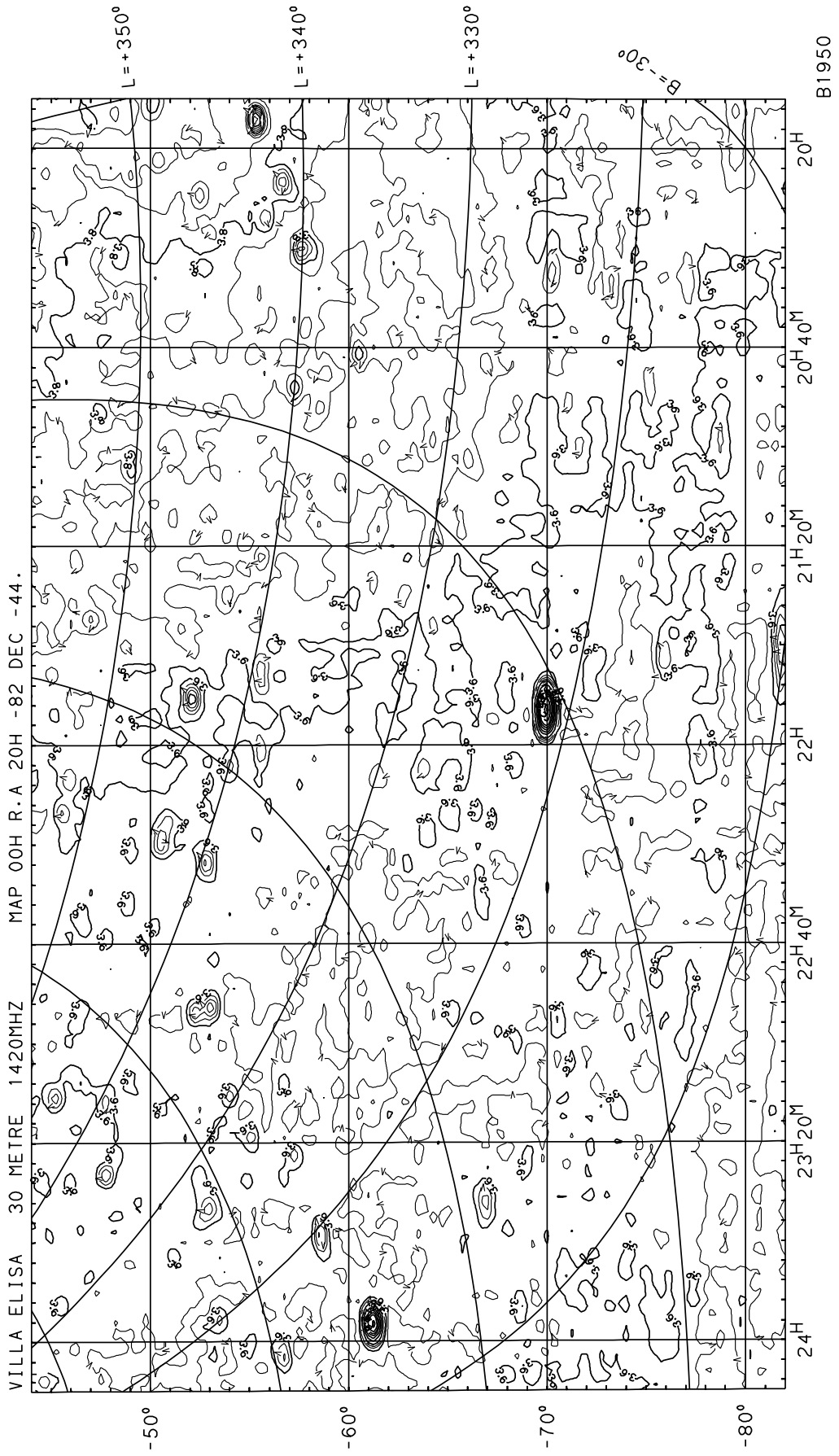
VILLA ELISA 30 METRE 1420MHZ MAP 00H R.A 20H -82 DEC -44.
L=+350°
L=+340°
L=+330°
B=-30°
B1950
20H
20H40M
21H20M
22H
22H40M
23H20M
24H
-50°
-60°
-70°
-80°

Fig. 1. l)

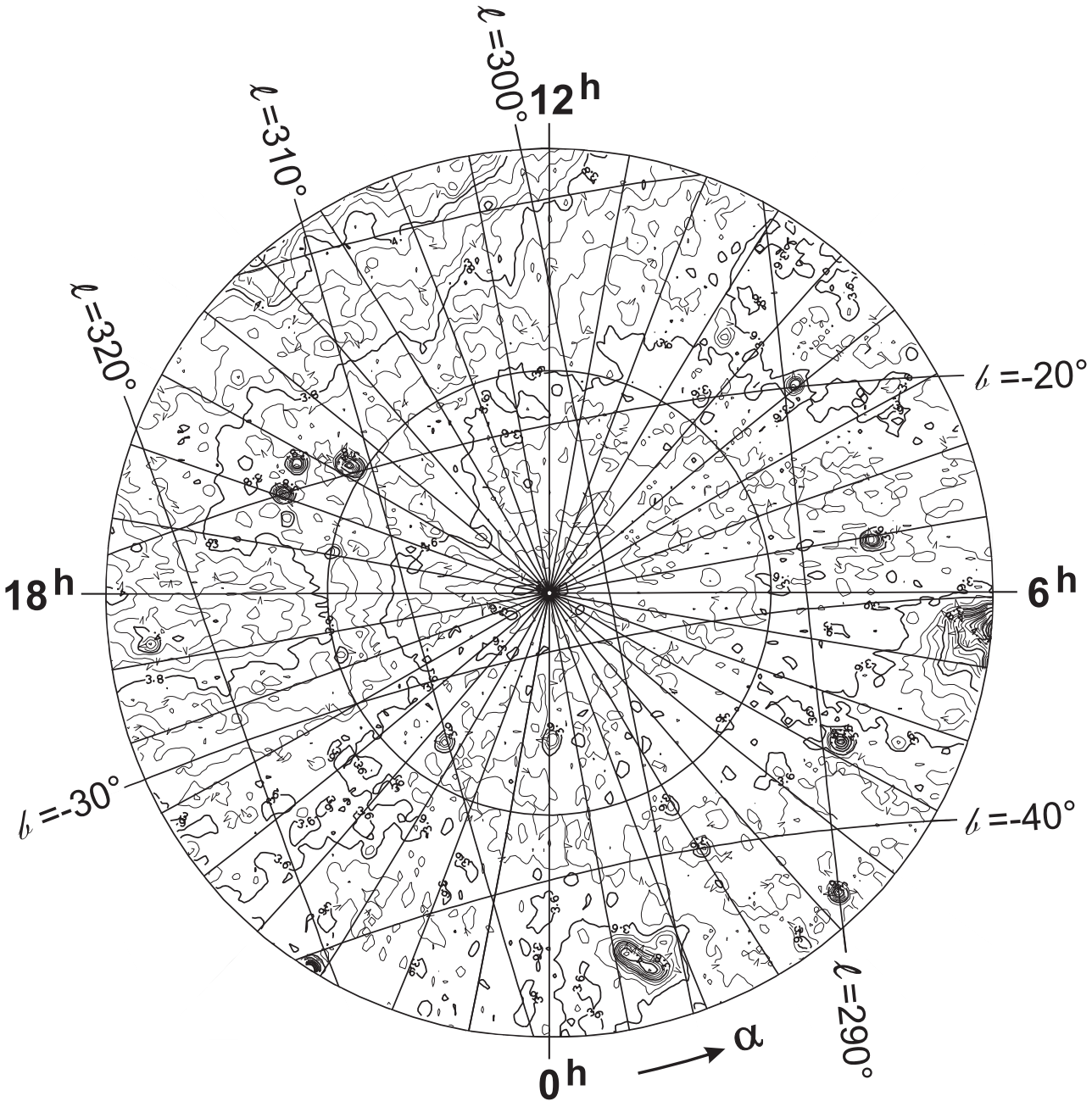

Fig. 2. Polar plot for declinations below −70°.

Full sets of contour maps transformed to B1950, J2000 or into Galactic coordinates can be obtained from `http://www.mpifr-bonn.mpg.de/survey/plots.html`.

4. Flux integration of discrete sources

4.1. Compact sources

Some peak flux densities of compact sources used for calibration have been included in Paper I, which have been tied to the main calibration sources used for the survey: Pictor A and Hydra A.

To further check the scale accuracy and the usefulness for measuring flux densities of sources from the survey maps we compared the integrated flux densities of a number of small-diameter sources with those measured with the Parkes 64-m telescope at the same frequency (PKSKAT90 – Wright & Otrupcek 1990). Picking up compact sources from the survey maps might be problematic since adjacent scans of the maps are observed on different nights with different residual pointing errors and calibration differences. The effect is that a slight broadening of compact sources cannot be ruled out. We have used two methods to find integrated flux densities. First we fitted elliptical Gaussians to the sources, and second we made ring integrations centered on the peak of the sources. The Parkes sources have flux densities which range from about 5 Jy to 250 Jy. Two stronger compact sources from the survey maps were added to compare the two

Table 2. Flux densities of selected compact sources in Jy.

Source Name	S(PKS)	S(Fit)	S(Int)
0043−424	8.1	7.4	6.9
0131−367	7.1	7.0	6.3
0252−712	5.9	4.7	4.4
0320−374	136.0	125.3	110.6
0407−658	14.4	13.1	12.0
0409−752	13.4	11.6	10.9
0518−458	66.0	55.4	53.3
0521−365	16.3	14.8	14.7
0634−205	6.0	9.1	
0822−428 Puppis A	128.0	129.5	101.9
0857−473 CTB31	250.0	248.1	232.0
0915−118 Hydra A	43.5	43.4	39.7
0922−517	30.0	32.6	30.6
1343−601	79.0	98.7	84.4
1610−771	4.6	4.7	
1637−771	5.8	4.9	4.5
1716−35		421.5	345.4
1721−34		659.0	605.4
1814−637	12.3	14.1	
1934−638	16.4	13.0	12.0
1932−464	12.6	10.7	9.7
1954−552	6.0	5.8	5.3
1938−155	7.0	6.9	6.3
2104−256	11.2	11.7	10.5
2152−699	30.0	26.4	23.9
2211−172	8.6	7.5	7.0
2356−611	22.0	21.4	20.3

integration methods. We list in Table 2 the flux densities from the Parkes telescope and those measured from the survey maps. Comparing Villa Elisa flux densities with those from the Parkes telescope for 25 sources results in a correlation coefficient of 0.99 ± 0.02 using method 1. Method 2 was successfully applied for 22 sources with the correlation coefficent of 0.90 ± 0.02. The flux densities listed in Table 2 were calculated by both methods assuming a Gaussian main-beam solid angle adapted from the northern sky survey of 1.27×10^{-4} sr or a $HPBW$ of $35\farcm4$. This is justified by the good matching of the southern sky maps with the maps from the nothern sky (see Paper I). However, a small but systematic difference in the two flux density integration methods is evident. The ring integration method should be less affected by the imperfect matching of adjacent scans, while the Gaussian fit tends to broaden the source size slightly. The ring integrated flux densities need a scaling by 1.11 to match the Parkes flux densities. Assuming the Parkes flux density scale is accurate this result indicates a slightly smaller main beam solid angle (1.14×10^{-4} sr) for the southern sky survey than for the northern sky (1.27×10^{-4} sr).

4.2. Extended sources

Flux density measurements of large-diameter objects in confused areas like in the Galactic plane or in regions with baselevel gradients or baselevel curvatures are difficult to perform and large uncertainties are unavoidable. The Large Magellanic Cloud (LMC) is located in an area of the sky which is not too highly affected. The LMC has been surveyed with the Parkes telescope at 1400 MHz by Haynes et al. (1986) with $15'$ angular resolution. The analysis of these data has been given by Klein et al. (1989), who obtained an integrated flux density of 529 ± 30 Jy for an area of $6\fdg2 \times 7\fdg5$ excluding compact sources in that field, which sum up for another 25 Jy. In total the Parkes flux density from the LMC area is 554 ± 30 Jy. We measure 584 ± 30 Jy including compact sources for the same area at 1420 MHz using a main-beam solid angle of 1.14×10^{-4} sr. Both flux densities agree within the errors. In this case baselevel uncertainties are small and are estimated to be of the order of 1% to 2% of the total flux.

The Small Magellanic Cloud (SMC) has been previously observed with the 30-m Villa Elisa telescope by Loiseau & Bajaja (1985), who calculated a flux density of 75 ± 5 Jy, which includes compact unrelated sources. Later Loiseau et al. (1987) corrected the flux density to 75 ± 10 Jy, which deviates largely from the derived 52 ± 5 Jy they found from Parkes observations. This discrepancy was attributed to different zero-level estimates. The Parkes value was obtained after subtraction of unrelated sources, which are estimated to contribute between 3.0 to 5.4 Jy. We measure 57 ± 3 Jy including compact sources after the subtraction of a smooth background. Our result agrees quite well with the Parkes flux density.

The giant radio galaxy Centaurus is located in the direction of a Galactic spur so that flux densities reported in the literature are difficult to interpret. Alvarez et al. (2000) give a reliable integrated flux density value of 1330 ± 133 Jy for the entire radio galaxy (derived from data of Cooper et al. 1965) at a frequency of 1410 MHz. We calculate a value of 1260 ± 65 Jy. Again this flux density agrees with the Parkes observations. These examples prove that reliable flux densities can be obtained for sources on all scales from the survey maps.

An analysis of the large Gum nebula area extending to about $40° \times 40°$ and its various thermal and nonthermal components was made by Testori (2001) and will not be repeated here.

5. Galactic foreground for the Cosmic Microwave Background

The all-sky survey at 408 MHz and the 1420 MHz northern sky survey are accessible via the web (`http://www.mpifr-bonn.mpg.de/survey.html`) in FITS-format. They have been used for a large number of investigations. Among these they are sometimes taken as "synchrotron templates" (which is a simplification, of course) to estimate the Galactic foreground contributions when studying fluctuations of the Cosmic Microwave Background (CMB). However, baseline distortion or "scanning effects" are clearly present in these

surveys, which might mask weak emission in cold regions at high Galactic latitudes where CMB data are collected.

Davies et al. (1996) presented a method explaining how to destripe the 408 MHz and the 1420 MHz survey maps in the Fourier plane. Despite this improvement they do not find these surveys useful for predictions of the Galactic high-latitude emission at higher frequencies. This result was based on a comparison with their low-resolution Tenerife sky-horn data at 10.4 GHz and 14.9 GHz. However, precise measurements at high frequencies are not easy. They may suffer from a low signal–to–noise ratio or some systematic deficits, as the agreement between the high-frequency scans is not perfect. Comparing different data sets in a suitable way is certainly of importance to identify problems of the individual data sets.

Recent discussions on the possible contribution of spinning dust emission with a spectrum peaking somewhere between 10 GHz and 30 GHz (de Olivera-Costa et al. 1998; Mukherjee et al. 2001) show that a simple extrapolation of low-frequency data is not appropriate, but that some modelling is required to get the high-frequency foreground. In this context it is of interest that the low-resolution 19 GHz all-sky map (Cottingham 1987; Boughn et al. 1992), which has 2 mK rms noise, is better correlated at high Galactic latitudes with the DIRBE all-sky maps at 100, 140 and 240 μm rather than with the 408 MHz all-sky map or the 1420 MHz northern sky map (de Olivera-Costa et al. 1998). Galactic synchrotron emission seems not to be the dominating emission component at high Galactic latitudes for frequencies above about 10 GHz.

6. Summary

We present the maps of the southern 1420 MHz radio continuum survey complementing the northern sky data to an all-sky survey at about $35\farcm4$ angular resolution. It has a slightly higher angular resolution compared to the 408 MHz all-sky survey of Haslam et al. (1982), but less resolution than the southern sky survey carried out by Jonas et al. (1998) at 2326 MHz with $20'$ ($HPBW$). This survey, on the other hand, has slightly less sensitivity compared to the 1420 MHz survey. The survey maps display the absolutely calibrated distribution of Galactic emission on all angular scales. The minimum of the emission is about 0.6 K above the extragalactic background which is seen towards the region around $l, b \sim 245°, +30°$. At the Galactic South Pole we measure +0.85 K. The survey is well suited to derive the spectral index distribution of the Galactic emission across the southern sky, which we will present in a forthcoming paper.

The angular resolution of the 1420 MHz survey matches that of the upcoming PLANCK mission in its lowest frequency channel at 31.5 GHz. We note that our sensitivity of 50 mK (3 × rms noise) for distinct steep-spectrum synchrotron features with $\beta = 3$ results in a signal of about 5 μK at 31.5 GHz, which is below the expected sensitivity of PLANCK (rms $\sim 20\,\mu$K) at that frequency. Also optically thin thermal features ($\beta = 2.1$) of 50 mK will have 8 μK at 31.5 GHz and thus are below the sensitivity limit. The 1420 MHz survey seems to be well suited to identify Galactic synchrotron and thermal features showing up in high-frequency maps observed with the aim studying the CMB.

Acknowledgements. We are indebted to Prof. R. Wielebinski for his support through all stages of the survey. J. C. T. wants to thank the Max-Planck-Gesellschaft for financial support during his stay at the MPIfR.

References

Alvarez, H., Aparici, J., May, J., & Reich, P. 2000, A&A, 355, 863
Berkhuijsen, E. M. 1972, A&AS, 5, 263
Boughn, S. P., Cheng, E. S., Cottingham, D. A., & Fixsen, D. J. 1992, ApJ, 391, L49
Cottingham, D. A. 1987, Ph.D. Thesis, Princeton University
Cooper, B. F. C., Price, R. M., & Cole, D. J. 1965, Aust. J. Phys., 18, 589
Davies, R. D., Watson, R. A., & Gutierrez, C. M. 1996, MNRAS, 278, 925
de Olivera-Costa, A., Tegmark, M., Page, L. A., & Boughn, S. P. 1998, ApJ, 509, L9
Haslam, C. G. T., Salter, C. J., Stoffel, H., & Wilson, W. E. 1982, A&AS, 47, 1
Haynes, R. F., Klein, U., Wielebinski, R., & Murray, J. D. 1986, A&A, 159, 22
Klein, U., Wielebinski, R., Haynes, R. F., & Malin, D. F. 1989, A&A, 211, 280
Loiseau, N., & Bajaja, E. 1985, Rev. Mexicana, 10, 95
Loiseau, N., Klein, U., Greybe, A., Wielebinski, R., & Haynes, R. F. 1987, A&A, 178, 62
Jonas, J. L., Baart, E. E., & Nicolson, G. D. 1998, MNRAS, 297, 977
Mukherjee, P., Jones, A. W., Kneissl, R., & Lasenby, A. N. 2001, MNRAS, 320, 224
Reich, P., & Reich, W. 1986, A&AS, 63, 205
Reich, P., & Reich, W. 1988, A&AS, 74, 7
Reich, W. 1982, A&AS, 48, 219
Reich, W., & Steffen, P. 1981, A&A, 93, 27
Tello, C., Villela, T., Smoot, G. F., et al. 2000, A&AS, 145, 495
Testori, J. C., Reich, P., Bava, J. A., et al. 2001, A&A, 368, 1123, Paper I
Testori, J. C. 2001, Ph.D. Thesis, Universidad Nacional de La Plata, Argentina
Wright, A., & Otrupcek, R. 1990, Bull. Inf. CDS, 41, 47 (PKSCAT90)